Simulation of thermoplastic 3D-printed parts for crash applications

Mathieu Vinot[1], Lars Bühler[1], Tobias Behling[1], Martin Holzapfel[1], Nathalie Toso[1]

[1] Institute of Structures and Design, German Aerospace Center, Stuttgart, Germany

1 Abstract

Keywords: additive manufacturing, thermoplastic material, numerical simulation, cohesive zone model

The rapid development of additive manufacturing techniques in aeronautic and automotive industry opens new possibilities in the design of metallic or composite parts compared to traditional subtractive processes. In particular, 3D printing allows the design of complex parts with a high lightweight potential through optimal use of material along the load paths. In the composite field, various printing techniques emerged in the last decade such as Selective Laser Sintering (SLS) or Fused Deposition Modelling (FDM) [1]. On the downside, 3D printing is confronted to the large influence of process parameters on the geometrical and optical quality as well as on the mechanical properties of the manufactured structures [2]. Moreover, simulation techniques with finite-element methods are still at their very beginning and improvements should be achieved to predict structural performances in crash applications.

Figure 1: SEAM manufacturing system from DLR

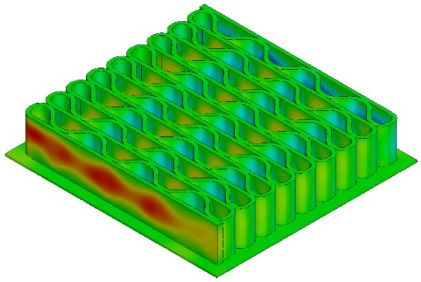

Figure 2: Deformation of a 3D-printed honeycomb structure under compressive loading

This paper focuses on the characterization and simulation of structures manufactured with the Screw Extrusion Additive Manufacturing (SEAM) technique presented in Figure 1. The material investigated is a combination of PA6 resin reinforced with 30% carbon fibres in weight. The mechanical behaviour under various loadings (tension, compression, shear) is first investigated in different material directions relative to the building direction with help of coupon specimens extracted from printed structures. The obtained properties are then fed in an anisotropic material card `*MAT157_ANISOTROPIC_ELASTIC_PLASTIC` and the respective performances studied by reproducing numerically the experimental tests. This contribution illustrates potential numerical solutions to recreate the mechanical behaviour between the printed layers and gives an insight into their advantages and drawbacks. Finally, an application of the suggested approach to generic honeycomb structures (Figure 2) is presented and the gaps in simulation technique are analysed.

2 Introduction

Additive manufacturing (AM) opened the door to new possibilities in term of structure design and customization. This technology has the ability to manufacture complex 3D geometries with high lightweight potential in absence of any mould or specific support tooling. Finally, AM can create parts on demand and therefore reduce the amount spare-parts which have to be stored on longer terms. Through the last 40 years, both hardware and software for AM has been evolving, getting faster and more accurate. In the field of AM with thermoplastic materials, there is still a need in a better comprehension and certification of the resulting materials and material properties for industrial application [3]. The strong dependency of the final mechanical properties to the manufacturing parameters and AM technique makes the structure sizing more complex. In particular, AM leads to a

strong anisotropic material behaviour and the properties of the interface between two layers is influenced by the material crystallinity, which depends itself directly on the manufacturing temperatures.
The present work is part of the DLR project “Fokusanwendungen, Fahrzeugstruktur, Antriebsstrang & Energiemanagement” (FFAE) [4] and contributes to improve the comprehension of AM thermoplastic materials through experimental testing and simulation. In this paper, a first detailed numerical approach is presented for the simulation of AM materials. The simulation is validated based on previously performed experimental tests on tensile specimens. Finally, the methodology is applied to a more complex generic structure under axial crushing.

3 Experimental test campaign

This chapter briefly presents the experimental tests performed for the material characterization and the analysis of failure mechanisms in 3D-printed materials. First, slices of the 3D-printed material are polished and the fibre orientation and length analysed with a Keyence VHX-5000 digital microscope (Figure 3). The polished micrographs in the building direction (in the part height) and the printing direction (along a strand) show a clear orientation of the short fibres along the printing direction in which 93 % (three sigma) of the fibres are oriented between 0° and 40°. The fibre length is measured on the rectangular fibre sections in the micrographs and has a mean value of 150 µm.

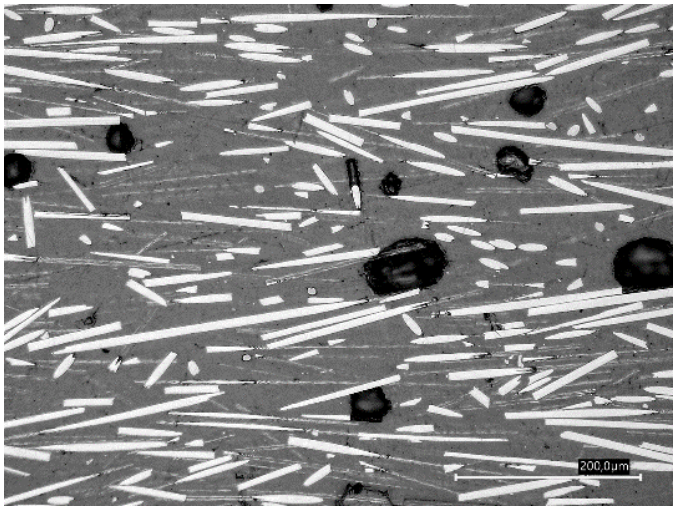

Figure 3: Visualization of the short fibres within the 3D-printed material captured on a polished micrograph sample

In a second step, flat tensile specimens are cut out of printed rectangular profile of 200 mm x 200 mm in 0°, 45° and 90° direction to the building direction. They are then tested under quasistatic conditions in a universal testing machine Zwick1494 to investigate the failure modes in the material and support the development of numerical solutions.

4 Simulation work

This chapter describes the modelling approach and the numerical solutions used for the simulation of 3D-printed materials. In a second part, the results at different simulation scales are presented.

4.1 Simulation approach

3D-printed structures can present complex, non-planar and strongly variating geometries and cannot be easily represented with classical thin-shell or thick-shell elements. Moreover, their anisotropic behaviour leads to the necessity of three-dimensional element formulations. The potential presence of small radii makes a meshing with a structured hexahedron mesh particularly complex and would require adequate meshing tools. For these reasons, the investigated specimens and parts are meshed layer by layer with 4-node tetrahedron elements ELFORM 13 for its simplicity of realisation and its sufficient accuracy compared to other formulations. The models presented in this paper are meshed with 1 mm elements in length and width. The element thickness is increased to combine several material layers (each layer is 0.5 mm thick) and reduce the computational time. The different virtual layers are represented by two alternating parts (see Figure 6) with merged nodes or with a contact formulation.

4.2 Simulation of material anisotropy

3D-printed materials present a strong material anisotropy caused by the strong orientation of the short fibres in the printing direction. Various material models, such as ***MAT054_ENHANCED_COMPOSITE_DAMAGE** or ***MAT058_LAMINATED_COMPOSITE_FABRIC** can consider orthotropic or anisotropic properties in LS-DYNA. However, the possibility to define material properties element wise with ***MAT157_ANISOTROPIC_ELASTIC_PLASTIC** is particularly suitable for 3D-printed parts, in which material properties can vary very locally depending on the printed geometry or the process parameters. In the present study, the material orientation within the ***MAT157** is defined for each element separately with the option AOPT = 0 and ***ELEMENT_SOLID_ORTHO**. The mechanical properties for the material card are extracted from the experimental tests from section 3 and sum up in Table 1.

Table 1: Generated material card *MAT157 for the PA6/CF material

MID	**RO**	**SIGY**	**LCSS**				
10	1.15e-6	0.053	10				
C11	**C12**	**C13**	**C14**	**C15**	**C16**	**C22**	**C23**
16.2	0.12	0.10	0	0	0	3.0	0.10
C24	**C25**	**C26**	**C33**	**C34**	**C35**	**C36**	**C44**
0.0	0.0	0.0	2.5	0.0	0.0	0.0	4.0
C45	**C46**	**C55**	**C56**	**C66**	**F**	**G**	**H**
0.0	0.0	3.0	0.0	2.4	22	0.5	0.5
L	**M**	**N**		**AOPT**			
77.0	77.0	77.0		0			

4.3 Simulation of damage and failure

The Tsai-Wu or Tsai-Hill failure criteria implemented in ***MAT157** are not accurate enough to describe precisely the anisotropic failure of 3D-printed material. The various failure modes such as local fibre axial failure, fibre pull-out, shear failure at the fibre/resin interface or resin failure by plasticization are homogenised in this work with the help of an anisotropic damage model ***MAT_ADD_GENERALIZED_DAMAGE**. This additional material card is an extension and a generalization of the well-known GISSMO damage model for the anisotropic failure and allow the definition of three damage models driven by user-defined history variables. In this work, the three principal components of the plastic strain rate tensor are the driving quantities for damage and damage accumulation is activated (DTYP = 1). To account for the influence of triaxiality on damage, a load curve is added for the variable LCSDG. The additional damage card is documented in Table 2 and the material response in a single element model under tension, compression and shear is illustrated in Figure 4.

Table 2: Generated additional failure card ***MAT_ADD_GENERALIZED_DAMAGE** for the carbon fibre reinforced PA6 material

MID	**IDAM**	**DTYP**	**REFSZ**	**NUMFIP**		**PDDT**	**NHIS**
10	1	1	1	1		3	3
HIS1	**HIS2**	**HIS3**	**IFLG1**	**IFLG2**	**IFLG3**		
0	0	0	1	1	0		
LCSDG	**ECRIT**	**DMGEXP**	**DCRIT**	**FADEXP**			
101		2.0	1.0	5.0			
LCSRS	**SHRF**	**BIAX**	**LCDLIM**	**MIDFAIL**	**NFLOC**		
			400				
…							

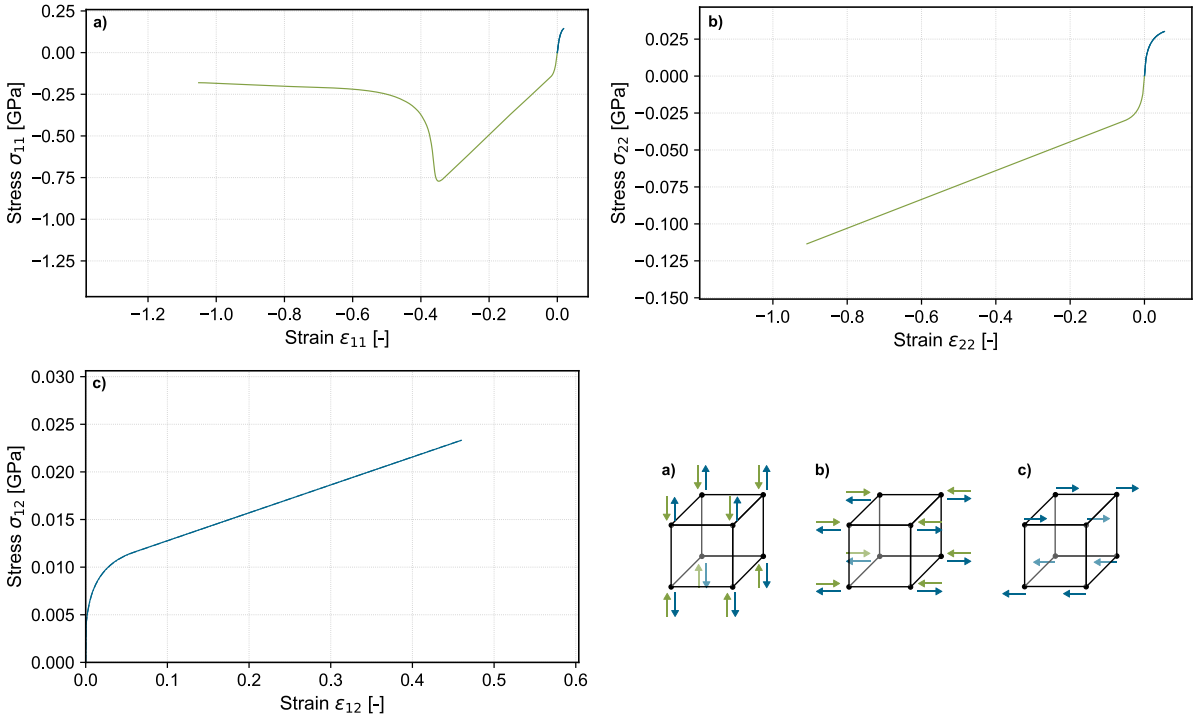

Figure 4: Mechanical behaviour of the pure PA6/CF material in a single element model with ***MAT_157** and ***MAT_ADD_GENERALIZED_DAMAGE**; the asymmetry between tension and compression results from different strains at failure and is no real material asymmetry with different yield strengths

The two material cards described previously only depict the behaviour of the sole intralayer material. The potential failure between two layers is reproduced using the cohesive contact ***CONTACT_AUTOMATIC_SURFACE_TO_SURFACE_TIEBREAK** with option 9. For this and to avoid high computational cost, a layer clustering is performed and the number of interfaces reduced. Table 3 sums up the material properties used as reference in this work. The latest contact formulation 13 with a trilinear traction-separation law could improve the modelling of interface failure in thermoplastic materials. However, no stable contact behaviour could be reached at the current time.

Table 3: Generated additional tiebreak contact for the interlayer failure in the carbon reinforced PA6 material

OPTION	NFLS	SFLS	PARAM	ERATEN	ERATES	CT2CN	CN
9	0.030	0.030	1.2	1.0e-4	1.0e-4	0.3	100

Finite-element models of the tensile specimens in 0°, 45° and 90° direction are generated and simulations performed for the reference interface properties of Table 3. Additionally, the interface strengths NFLS and SFLS are varied to investigate their influence on the mechanical properties of the three material directions (Figure 5). The simulation with ***MAT157** reproduces well the results from the 0° and 90° specimens but underestimate the strengths in the 45°direction. The interface strengths have no influence on the strength of the 0° specimen. This estimation is in good agreement with test results, as no interface failure has been observed for this loading angle. The mechanical specimen strength in 45° and 90° direction is linearly increasing with the interface strength. An interface strength similar to the strength of the intralayer material results in a mixed specimen failure with layer decohesion and intralayer failure (Figure 6). Below this value, the specimen is failing through total decohesion. This dependency of material failure to the interface strength is of particular importance for the structural sizing.

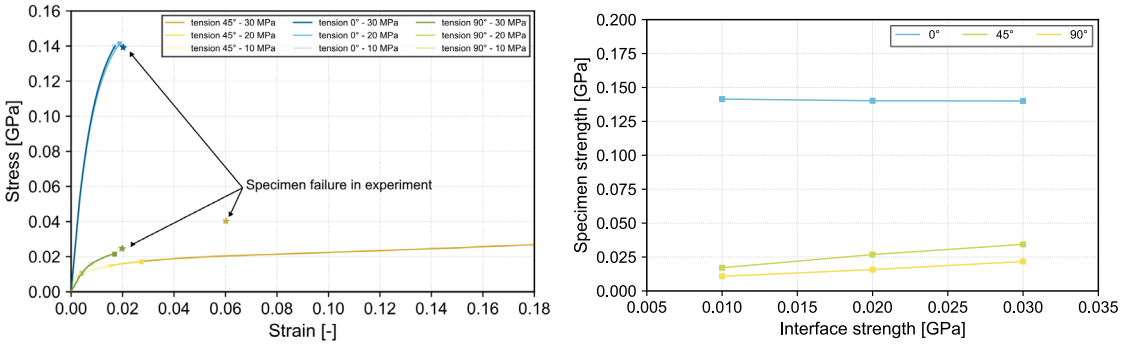

Figure 5: Stress versus strain curves (left) and evolution of the mechanical properties (right) in the 0°, 45° and 90° samples as a function of the interface strength

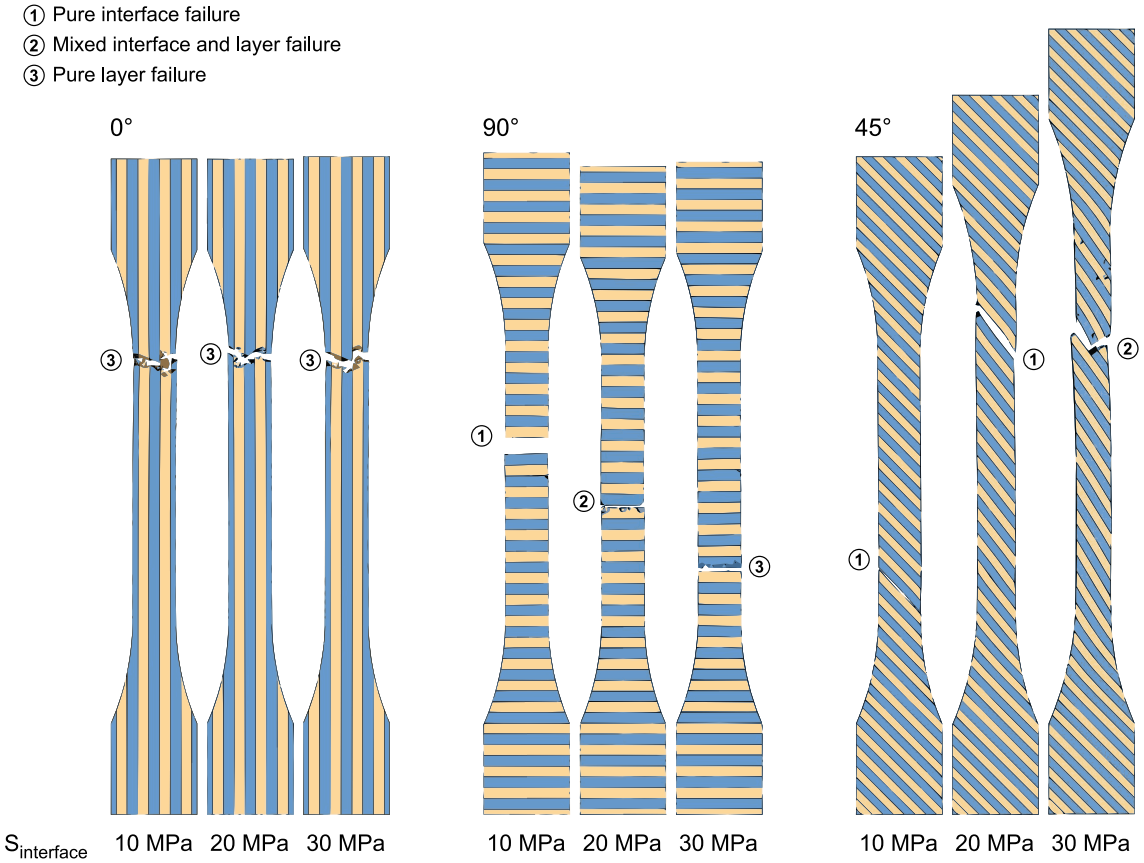

Figure 6: Influence of the interface strength on the failure patterns of tensile specimens under 0°, 45° and 90° loading

4.4 Application on a 3D-printed profile

The material card and contact formulation are finally applicated to the example of a generic 3D-printed specimen loaded under axial crushing (Figure 7b). On this level, the influence of the interface strength on the specific energy absorption is investigated. The finite-element model of the crushing profile is automatically generated using the slicing result for the part manufacturing (G-Code). First, the spaces between the control nodes of the G-Code are refined for a user-defined element length (Figure 7a). Assuming a constant width of the strands, the part outer and inner contour is then calculated. In a last step, the closed profile is meshed with 2D-triangular elements. At this step, the path orientation based on the G-Code is attributed locally to each element via **`*ELEMENT_SOLID_ORTHO`**. The resulting mesh can then be extruded in the height to create the printed layers. To reduce the computing time, several layers are combined into one thicker layer depending on the simulation strategy and wanted level of detail required.

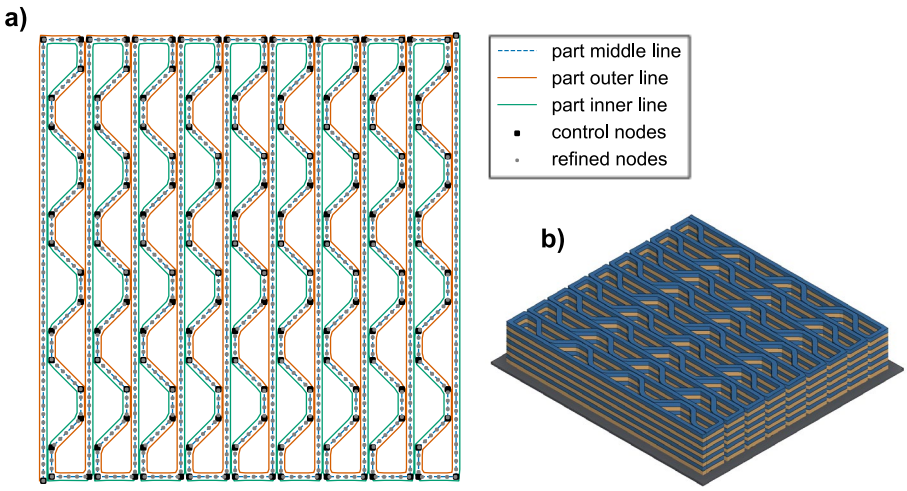

Figure 7: a) Modelling technique based on a G-Code and resulting mesh b) for a crushing profile

In the following, the advantages of the developed approach and of the use of a generalized damage model are investigated and compared to a material card ***MAT058** with similar material properties. The results are then compared to experimental results from [5]. The material model ***MAT157** underestimates the reaction force in the specimen (Figure 8). This is due to the absence of tension-compression asymmetry in this material card compared to the ***MAT058** and as a consequence to the impossibility to depict both tension and compression loading correctly with a same material card. On the contrary, the ***MAT058** depicts the maximal compression force more accurately but does not simulate the correct damage behaviour in the specimen. The appending of *MAT_ADD_GENERALIZED_DAMAGE does not improve the force versus displacement curve much.

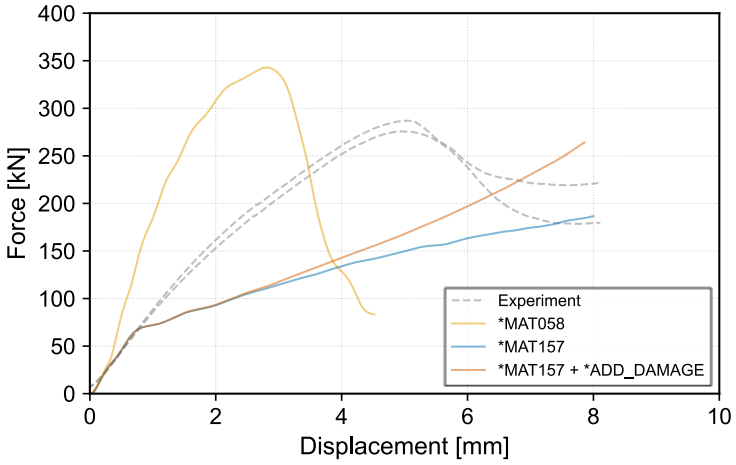

Figure 8: Force versus displacement curves in experiment and in simulation with *MAT157, *MAT157 + *MAT_ADD_GENERALIZED_DAMAGE and *MAT058

However, the failure patterns using the anisotropic damage model are closer to these observed in experiment (Figure 9). Due to the compressive load, the flanges and outer webs of the specimen are buckling and subsequently failing under bending loading (Figure 9a). In simulation, the inner webs are not kinking as observed in the experimentally tested specimen (Figure 9b). This can be explained by the defects brought in the structure during the printing, which weaken the part and reduce its stability under compression loading. The model with *MAT058 fails suddenly under pure compression in the profile's mid-section (Figure 9d). With this material model, no instability is visible in the simulated profile and the use of **SLIM** values leads to a pure compression loading in the profile (Figure 9c).

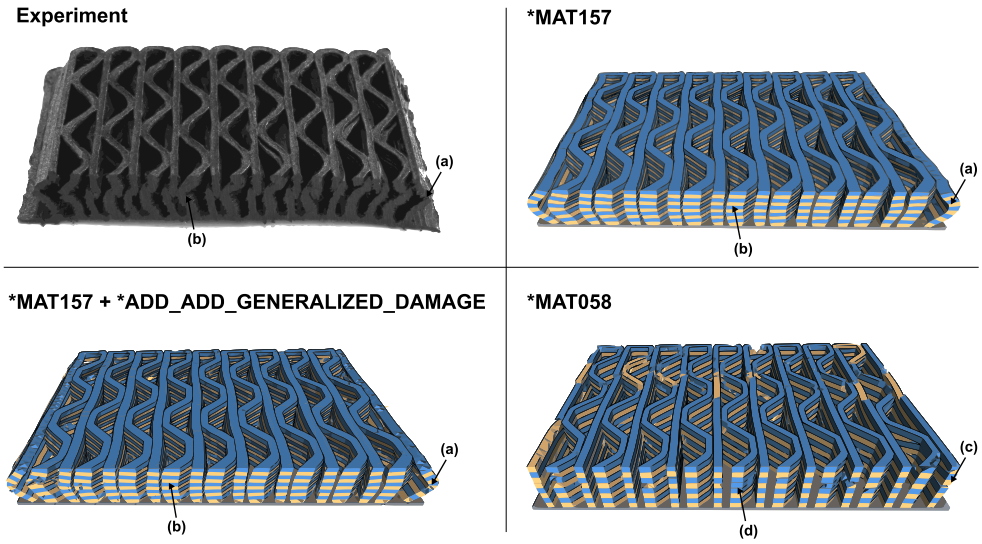

Figure 9: Failure patterns in the specimen under axial crushing in experiment and simulation

5 Conclusion and outlook

In the present contribution, a numerical approach has been developed to reproduce the anisotropic behaviour of short fibre reinforced thermoplastic 3D-printed materials. The intralayer behaviour has been modelled by the combination of an anisotropic material model **`*MAT157`**, the element wise attribution of material orientation and an anisotropic damage and failure model **`*MAT_ADD_GENERALIZED_DAMAGE`**. The interlayer behaviour and failure were depicted by a cohesive contact. With this approach, the first simulation results are able to predict the influence of the interface strength on the global material performances on the specimen level. The results highlighted the importance of increasing the interface strength to reach optimal mechanical properties in 3D-printed material. However, the chosen approach revealed insufficient to model the crushing behaviour in a printed profile. While the overall behaviour benefited from the anisotropic damage model, the reaction force in the profile could not be accurately simulated. In comparison to *MAT058, *MAT157 recreates more precisely the failure patterns in the 3D-printed material,
The complexity of 3D-printed material however requires further development of the modelling and simulation methodology. In particular, the variability and scatter in the layers' geometry and their positioning relatively to each other can play a critical under specific loadings such as compressive loading or crushing. Finally, the simulation should be improved to consider locally variable mechanical properties resulting from the manufacturing process. To this purpose, mapping approaches from process simulation could reveal helpful.

Acknowledgment

This work was funded by the German Aerospace Center within the project FFAE Fokusanwendungen, Fahrzeugstruktur, Antriebsstrang & Energiemanagement.

Literature

[1] A. Jandyal, I. Chaturvedi, I. Wazir and M. I. U. H. A. Raina, "3D printing – A review of processes, materials and applications in industry 4.0," Sustainable Operations and Computers Vol. 3, pp. 33-42, 7 October 2021.
[2] M. Pivar, D. Gregor-Svetec and D. Muck, "Effect of Printing Process Parameters on the Shape Transformation Capability of 3D Printed Structures," Polymers Vol. 14, 29 December 2021.
[3] McKinsey & Company, https://www.mckinsey.com/capabilities/operations/our-insights/the-mainstreaming-of-additive-manufacturing, 17 July 2023.
[4] Deutsches Zentrum für Luft- und Raumfahrt e.V., https://verkehrsforschung.dlr.de/de/projekte/ffae-fokusanwendungen-fahrzeugstruktur-antriebsstrang-energiemanagement, 17 Juli 2023.
[5] L. Bühler, „Experimentelle und numerische Untersuchung des mechanischen Werkstoffverhaltens von 3D-gedruckten Materialien für Crash-Anwendungen", German Aerospace Center, 2022.